

# Anatomy of Bond Formation. Domain-Averaged Fermi Holes as a Tool for the Study of the Nature of the Chemical Bonding in $\text{Li}_2$ , $\text{Li}_4$ , and $\text{F}_2^\dagger$

Robert Ponec\*

*Institute of Chemical Processes Fundamentals, Czech Academy of Sciences, Prague 6, Suchbát 2, 165 02, Czech Republic*

David L. Cooper

*Department of Chemistry, University of Liverpool, L69 7ZD Liverpool, U.K.*

*Received: January 31, 2007; In Final Form: May 2, 2007*

Domain-averaged Fermi hole (DAFH) analysis represents a relatively new strategy for extracting useful new insights into electronic structure and bonding from correlated wave functions. We analyze a full-valence CASSCF description of the  $\text{Li}_4$  rhombus, in order to discern the role played by the domains of the non-nuclear attractors in the sharing of the valence electrons. Similarly we examine the electron reorganization that accompanies the bond dissociation process in the  $\text{Li}_2$  molecule, which also features such a non-nuclear attractor for a significant range of nuclear separations. Full-CI wave functions for  $\text{H}_2$ , for a wide range of bond lengths, are used to determine how robust are the DAFH descriptions from full-valence CASSCF wave functions to the incorporation of dynamical electron correlation. Comparisons are made, for  $\text{H}_2$  and  $\text{Li}_4$ , with a much cheaper strategy in which restricted Kohn–Sham orbitals from B3LYP calculations are inserted into a simplified DAFH expression which applies at the restricted Hartree–Fock level. We also investigate the breaking of the relatively weak F–F bond in  $\text{F}_2$ , in order to determine the extent to which the DAFH analysis of such a system differs from that of a more conventional homopolar bond, such as the one in  $\text{H}_2$ .

## 1. Introduction

As is well-known, tools in widespread use for analyzing arbitrary correlated wave functions (or electron densities) include atoms in molecules (AIM),<sup>1</sup> ELF,<sup>2</sup> NBO,<sup>3</sup> various families of population analysis and bond orders, and a range of energy decomposition schemes. A recent addition to this toolbox is domain-averaged Fermi hole (DAFH) analysis, which aims to extract highly visual information about the electronic structure and bonding from (correlated) one- and two-particle density matrices. The methodology has been successfully used with CASSCF and modern-VB correlated wave functions to investigate the bonding in  $\text{CH}_4$ ,  $\text{CH}_2\text{N}_2$ , and  $\text{CH}_2\text{Li}_2$  near equilibrium geometry as well as the geometry dependence of the bonding in  $\text{H}_2$ ,  $\text{LiH}$ , and  $\text{N}_2$ .<sup>4</sup> Further insight, especially into the bond dissociation process, has been provided by a numerical quantity which we call the shared-electron distribution index (SEDI).<sup>4,5</sup> As currently implemented, the chosen domains for DAFH (and SEDI) analysis of correlated wave functions are those that arise in AIM partitioning of the total electron density.

The purpose of the present work is to seek answers to a number of questions that have been raised by our previous study. The main issues to be addressed here are as follows:

1. An interesting feature of various species, such as lithium clusters, is the existence of non-nuclear attractors (NNAs) in the total electron density.<sup>6,7</sup> It remains to be seen how the presence of such NNAs influences the description of the bonding that is revealed by DAFH analysis and SEDI values, and so we examine here the  $\text{Li}_4$  rhombus near its equilibrium geometry and the geometry dependence of the bonding in  $\text{Li}_2$ .

2. Prior to our recent work,<sup>4</sup> DAFH analysis had previously been applied within a simplified formulation, valid at the restricted Hartree–Fock (RHF) level, that avoids the need for the two-particle density matrix.<sup>8</sup> This simplified formulation, requiring instead only the doubly occupied orbitals, had been applied to a wide variety of systems using either RHF orbitals or restricted Kohn–Sham (RKS) orbitals. We compare here, for  $\text{H}_2$  and for  $\text{Li}_4$ , the RHF and pseudo-RKS levels of DAFH analysis with results based on correlated density matrices.

3. DAFH analysis based on correlated density matrices has mostly been applied to wave functions that take into account nondynamical correlation. We examine here the geometry dependence of the description of the bonding in  $\text{H}_2$  utilizing a wave function that also takes into account dynamical correlation. Indeed, we use the exact solution (within the given basis set) of the usual clamped-nucleus Schrödinger equation.

4. The relatively low dissociation energy of the  $\text{F}_2$  molecule suggests that the bonding in this molecule could be somewhat different from the more ordinary covalent bonds in other homopolar systems. It remains to be seen to what extent, if at all, DAFH analysis can distinguish the bonding in  $\text{F}_2$  from that in (say)  $\text{H}_2$ . Accordingly, we examine here the electron reorganization during the splitting of the F–F bond.

## 2. Theoretical

The most straightforward way of introducing the idea of domain-averaged Fermi holes (DAFH) is via selective integration of the so-called correlation function  $C(\mathbf{r}_1, \mathbf{r}_2)$ ,<sup>9</sup> defined in terms of the (spinless) pair density  $\rho(\mathbf{r}_1, \mathbf{r}_2)$  and

<sup>†</sup> Part of the “Thom H. Dunning, Jr., Festschrift”.

\* Corresponding author e-mail: rponec@icpf.cas.cz.

the one-electron density  $\rho(\mathbf{r}_1)$ :

$$C(\mathbf{r}_1, \mathbf{r}_2) = 2\rho(\mathbf{r}_1, \mathbf{r}_2) - \rho(\mathbf{r}_1)\rho(\mathbf{r}_2) \quad (1)$$

Integration (averaging) over a finite domain  $\Omega_B$  yields the domain-averaged Fermi hole:

$$g_B(\mathbf{r}_1) = - \int_{\Omega_B} C(\mathbf{r}_1, \mathbf{r}_2) d\mathbf{r}_2 = \rho(\mathbf{r}_1) \int_{\Omega_B} \rho(\mathbf{r}_2) d\mathbf{r}_2 - 2 \int_{\Omega_B} \rho(\mathbf{r}_1, \mathbf{r}_2) d\mathbf{r}_2 \quad (2)$$

In principle, the form of the domain  $\Omega_B$  could be completely arbitrary, but it has been shown in a number of studies at the RHF and pseudo-RKS levels,<sup>8</sup> and by our recent study using correlated pair densities,<sup>4</sup> that interesting and relevant information for structure elucidation can be extracted when the domains are identified with those resulting from AIM partitioning of the total electron density.

In the present work, the integration over AIM domains that is required for the DAFH analysis (and the generation of SEDI values) was performed using the PROAIMV program (Version 94 Revision B). The quantities extracted from PROAIMV are the so-called AOM matrices for each domain. These are simply the (symmetric) matrices of overlaps between the orthonormal natural orbitals, but with the integrations restricted to the relevant domain. The sum of the AOM matrices for all domains should, of course, correspond to a unit matrix.

The required density matrices, and thus  $g_B(\mathbf{r}_1)$ , were expressed in the natural orbital basis which diagonalizes the usual one-particle density matrix. An isopycnic transformation<sup>10</sup> of the eigenvectors and eigenvalues of  $g_B(\mathbf{r}_1)$ , which leaves  $g_B(\mathbf{r}_1)$  unchanged, results in the one-electron functions  $f_i$  and corresponding occupation numbers  $\epsilon_i$  on which the DAFH analysis is based.

Further selective integration of  $g_B(\mathbf{r}_1)$  over a finite domain  $\Omega_A$ , as in eq 3, provides a quantitative measure of the extent of electron sharing between AIM atomic domains  $\Omega_A$  and  $\Omega_B$ .

$$k(A, B) = \int_{\Omega_A} g_B(\mathbf{r}_1) d\mathbf{r}_1 \quad (3)$$

We may then define the shared-electron distribution index (SEDI) according to

$$\text{SEDI}(A, B) = k(A, B) + k(B, A) \quad (4)$$

SEDI is much the same quantity as the so-called delocalization index that was introduced by Bader and co-workers.<sup>11</sup> As was pointed out in our previous work,<sup>4,5</sup> we much prefer the name shared-electron distribution index (SEDI) to ‘delocalization index’, mostly because it is so much more descriptive and it also avoids possible confusion with a range of alternative measures of the degree of delocalization. We do, however, retain the name ‘localization index’ for the intradomain terms,  $k(A, A)$ .<sup>11</sup>

Unlike the conditional pair density for same-spin electrons,<sup>12,13</sup> all of the quantities examined here are spinless. It would, however, be fairly straightforward to perform separately the same-spin and different-spin DAFH (and SEDI) analysis if the required spin-dependent pair density matrices were available for correlated wave functions. This is something that we are currently pursuing. In this context, we much prefer the use of the actual density matrices for correlated descriptions to schemes that rely on approximations that become exact at the RHF level.<sup>14</sup>

### 3. Computational Details

For H and F atoms, we used the contracted Cartesian Gaussian basis sets of triple- $\zeta$  valence plus polarization quality which

are stored internally in GAMESS-UK<sup>15</sup> as TZVP and in MOLPRO<sup>16</sup> as GAMESS-PVTZ. These basis sets are derived from the work of Dunning.<sup>17</sup> Given that no analogous basis set for Li is stored internally in those packages, we went back to Table 5 of the original paper by Dunning<sup>17</sup> and adopted his [4s] contraction of a (10s) primitive set, which we augmented with a single p function on Li with an exponent of 0.17.

CASSCF wave functions were calculated for H<sub>2</sub>, Li<sub>2</sub>, Li<sub>4</sub>, and F<sub>2</sub> in  $D_{2h}$  symmetry using the MOLPRO package,<sup>16</sup> from which we can extract the required one- and two-particle spinless density matrices, expressed in the natural orbital basis. For the purposes of comparison, we also carried out various RHF and RKS calculations, using for the latter the conventional B3LYP functional that is known in MOLPRO by the alias ‘b3lyp3’.<sup>16</sup>

In the case of H<sub>2</sub>, the chosen basis set is sufficiently compact that it is practical to carry out 2 electrons in 12 orbitals CASSCF calculations which correspond to a full CI in this basis set. We considered a range of internuclear distances from 0.5 to 3 Å.

For Li<sub>2</sub> we carried out 2 electrons in 8 orbitals full-valence CASSCF calculations for a range of bond lengths from 2.0 to 4.5 Å, whereas in the case of Li<sub>4</sub> we carried out the analogous full-valence CASSCF (4 electrons in 16 orbitals) for a planar rhombus geometry. Each side of the rhombus is 5.552 bohr, with the shortest distance across the ring (Li<sub>1</sub>...Li<sub>2</sub>) of 4.936 bohr.<sup>18</sup>

Calculations on F<sub>2</sub> were carried out for a range of bond lengths from 1.25 to 2.50 Å. Mostly for consistency with the treatments of Li<sub>2</sub> and Li<sub>4</sub>, we again adopted the full-valence CASSCF prescription, which corresponds in this case to distributing 14 electrons in just 8 orbitals. This is a relatively low-level of theory for this molecule, but it should be more than adequate to highlight the differences from H<sub>2</sub>.

Although the various integrations in eqs 2 and 3 are, of course, over the AIM domains defined by partitioning of the *total* electron density, all of the subsequent analysis presented in this paper is exclusively for the valence electrons. We have checked for systems such as those described here that there are no important differences in the interpretation of SEDI or DAFH between all-electron and valence-only analyses.

### 4. Results and Discussion

**H<sub>2</sub>.** Before discussing the peculiarities of the bonding in the Li<sub>4</sub> cluster and in the Li<sub>2</sub> and F<sub>2</sub> molecules, it is useful to analyze first the full-CI results for the ordinary two-center two-electron bond in H<sub>2</sub>. For all of the bond lengths considered, from 0.5 to 3 Å, DAFH analysis for a hydrogen atom in H<sub>2</sub> yields one dominant occupation number,  $\epsilon_1$ , that is close to unity. We find that the numerical values of  $\epsilon_1$  for larger nuclear separations  $R$  are practically the same as those from our previous 2 electrons in 2 orbitals CASSCF calculations in the same basis set.<sup>4</sup> At shorter  $R$ , the current full-CI values are slightly lower than those from the smaller calculation, but the differences are fairly small. For example, the value of  $\epsilon_1$  for  $R = 1$  Å drops from 0.994 to 0.991, and that for 0.5 Å drops from 0.998 to 0.993. The forms of the corresponding functions  $f_1$  (see Figure 1) are much the same as those reported in our previous work.<sup>4</sup> For shorter  $R$ ,  $f_1$  is reminiscent of the  $1\sigma_g$  molecular orbital of H<sub>2</sub>, delocalized over both atoms, whereas elongation of the bond results in increased localization onto the H atom for which the analysis was performed, so that the function takes the form of H(1s) at dissociation. We can conclude for this system that the inclusion of dynamical electron correlation makes only small quantitative differences to the DAFH analysis relative to the corresponding

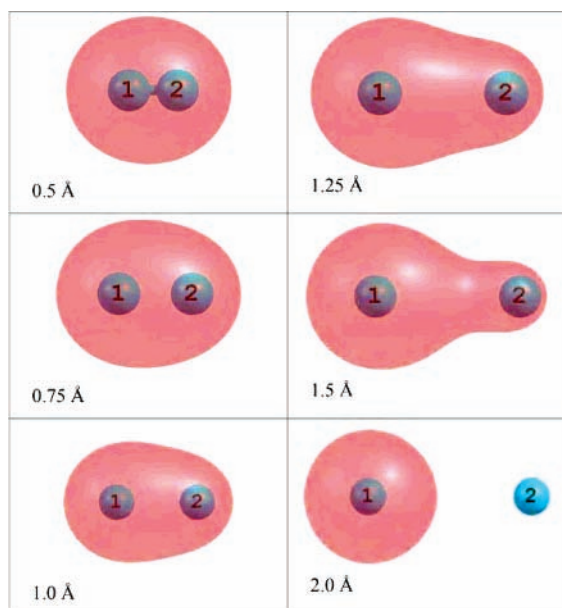


**Figure 1.** Dissociation of the H–H bond monitored by the  $R$ -dependence of DAFH eigenvectors associated with the domain of a hydrogen atom in  $H_2$ .

treatment that includes only nondynamical correlation, but the basic description is otherwise much the same.

At the RHF level, the spinless two-particle density matrix expressed in the MO basis takes the particularly simple form shown in eq 5.

$$D(ij|kl) = 2\delta_{ik}\delta_{jl} - \delta_{il}\delta_{jk} \quad (5)$$

Given this expression, it is then very straightforward to show that the matrix to be diagonalized for the DAFH analysis of a given AIM domain is simply twice the corresponding AOM matrix. In the case of an RHF description of  $H_2$ , with its single doubly occupied  $\sigma_g$  orbital, the AOM matrix for either domain consists of a single element equal to 0.5. As a consequence, the matrix to be diagonalized is just a  $1 \times 1$  unit matrix, thus giving us an eigenvalue of unity and an eigenvector that is simply the  $\sigma_g$  orbital. This argument shows us that DAFH analysis of an RHF description of  $H_2$  becomes increasingly untenable as the bond dissociates. This is, of course, a direct consequence of the failure of the RHF model to provide a realistic description of such a bond-breaking process.

The simplification that the matrix to be diagonalized is twice the AOM matrix relies on eq 5. However, if one simply assumes that it is reasonable to use the same ‘trick’ but with RKS orbitals, then it is straightforward to perform what we have called ‘pseudo-RKS’ DAFH (and SEDI) analysis. It follows, though, if the single doubly occupied orbital again has  $\sigma_g$  symmetry, that DAFH analysis in the case of  $H_2$  will necessarily return that  $\sigma_g$  orbital. This argument is entirely independent of bond length, but it is clear (just as for the RHF case) that such an outcome will become increasingly untenable as the bond dissociates. Inserting RKS orbitals into the simplified expression that applies for the RHF level certainly does not take proper account of correlation effects. Nonetheless, a variety of quantities continue to be presented in the literature based on such ‘pseudo-RKS’ simplifications without appropriate warnings about their (obvious) limitations.

**Li<sub>4</sub>.** For all of the levels of theory we have considered here, AIM analysis of the total electron density detects the presence of one non-nuclear attractor (NNA) in each of the  $Li_1Li_2Li_3$

**SCHEME 1: Numbering Scheme for the Lithium Atoms and the NNAs in the  $Li_4$  Rhombus**

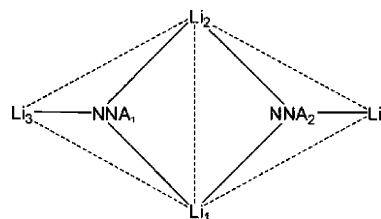


**TABLE 1: Valence Electron Populations ( $q$ ), Shared-Electron Distribution Indices (SEDI), and Localization Indices ( $k$ ) for AIM Domains in the  $Li_4$  Rhombus, as Calculated at the Full-Valence CASSCF, B3LYP, and RHF Levels of Theory<sup>a</sup>**

	CASSCF	B3LYP	RHF
$q(Li_1)$	0.206	0.205	0.165
$q(Li_3)$	0.643	0.626	0.585
$q(NNA_1)$	1.151	1.169	1.250
SEDI( $Li_1, Li_2$ )	0.012	0.027	0.017
SEDI( $Li_1, Li_3$ )	0.037	0.046	0.037
SEDI( $Li_3, Li_4$ )	0.070	0.114	0.082
SEDI( $Li_1, NNA_1$ )	0.139	0.132	0.111
SEDI( $Li_3, NNA_1$ )	0.565	0.602	0.622
SEDI( $Li_3, NNA_2$ )	0.023	0.064	0.058
SEDI( $NNA_1, NNA_2$ )	0.168	0.158	0.166
$k(Li_1, Li_1)$	0.024	0.014	0.009
$k(Li_3, Li_3)$	0.279	0.190	0.167
$k(NNA_1, NNA_1)$	0.634	0.626	0.716
$\epsilon_1(Li_1)$	0.111 (2 $\times$ )	0.103 (2 $\times$ )	0.083 (2 $\times$ )
$\epsilon_1(Li_3)$	0.615 (1 $\times$ )	0.615 (1 $\times$ )	0.578 (1 $\times$ )
$\epsilon_1(NNA_1)$	1.003 (1 $\times$ )	1.117 (1 $\times$ )	1.195 (1 $\times$ )
	0.059 (1 $\times$ )	0.052 (1 $\times$ )	0.055 (1 $\times$ )
	0.041 (1 $\times$ )		
	0.035 (1 $\times$ )		
SEDI( $\Omega_\alpha, \Omega_\beta$ )	0.283	0.399	0.364

<sup>a</sup> Also listed are the corresponding numerical values and degeneracies of the occupation numbers (transformed eigenvalues)  $\epsilon_i$  from the DAFH analysis.  $\Omega_\alpha \equiv Li_3NNA_1$  and  $\Omega_\beta \equiv Li_4NNA_2$ . Note that all of the values for the B3LYP case other than populations are based on a simplification that applies at the RHF level, as discussed in the text.

and  $Li_1Li_2Li_4$  triangles, as is illustrated in Scheme 1. Such a pattern of NNAs does, of course, closely resemble those found in previous work.<sup>6</sup> The populations of individual AIM domains of this cluster are summarized in Table 1 for the valence electrons. As is to be expected, the B3LYP and full-valence CASSCF values are the most similar, because of the relative qualities of the different electron densities. The changes to the distance between the NNAs (RHF=4.99 bohr, B3LYP=4.78 bohr, CASSCF=4.82 bohr) are fairly small, and the corresponding populations lie within the range 1.15–1.25. Any significant differences between the DAFH analyzes at the RHF and CASSCF levels will have very much more to do with the character or flexibility of the wave functions than with changes to the positions or shapes of the NNA domains.

The numerical values and degeneracies of the occupation numbers (transformed eigenvalues)  $\epsilon_i$  from the DAFH analysis of the valence electrons of the RHF and full-valence CASSCF wave functions are reported in Table 1, and the corresponding symmetry-unique one-electron functions  $f_i$  are displayed in Figure 2. The main difference in the form of these functions for the different levels of theory is observed for the domain of atom  $Li_1$  (and  $Li_2$ ). Whereas the RHF treatment apparently lacks sufficient flexibility to allow the sets of functions for these two domains to be different from one another, the corresponding symmetry-equivalent sets at the full-valence CASSCF level are seen to be associated with different ‘sides’ of the rhombus. On

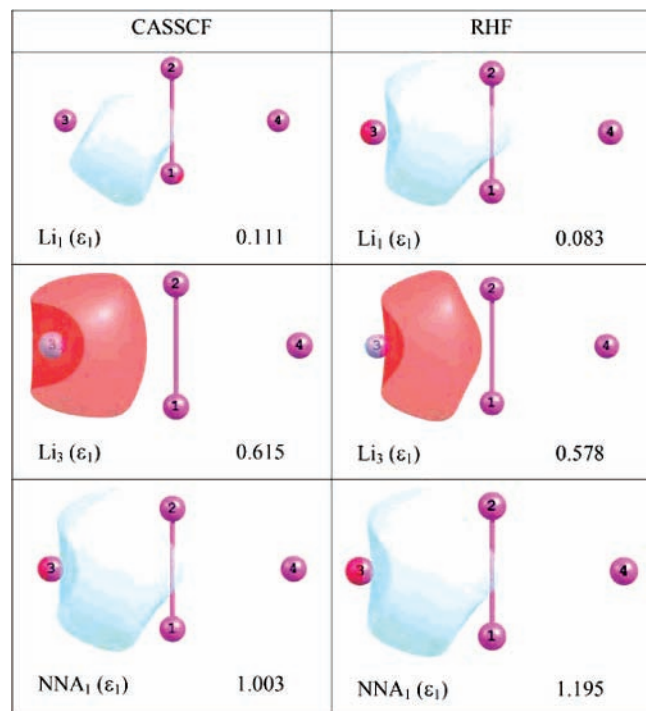


**Figure 2.** Comparison of symmetry-unique DAFH eigenvectors associated with AIM domains of the Li<sub>4</sub> cluster, as generated at the full-valence CASSCF and RHF levels of theory.

the other hand, the shapes of the functions associated with the larger occupation numbers for atom Li<sub>3</sub> (and Li<sub>4</sub>) and non-nuclear attractor NNA<sub>1</sub> (and NNA<sub>2</sub>) are not so different from RHF to full-valence CASSCF. For both levels of theory, the forms of these functions (and the dominance of the corresponding occupation numbers) are suggestive of multicenter bonding within the individual Li<sub>1</sub>Li<sub>2</sub>Li<sub>3</sub>NNA<sub>1</sub> and Li<sub>1</sub>Li<sub>2</sub>Li<sub>4</sub>NNA<sub>2</sub> subunits.

Although the main features of the nature of the bonding in this cluster are revealed by the DAFH functions  $f_1$  associated with the dominant occupation numbers,  $\epsilon_1$ , further insight is provided by the existence of additional functions for the NNAs which are associated with the small, but not negligible, occupation numbers listed in Table 1. The most important function in this respect is  $f_2$ , associated with  $\epsilon_2$  values of 0.059 and 0.055 for the CASSCF and RHF wave functions, respectively. As can be seen from Figure 3, the form of this function is in all cases reminiscent of the dominant NNA eigenvector except that it is localized in the region of the adjacent lithium triangle, consistent with our notions of the interfragment sharing of electrons. In the case of the CASSCF calculations, there is also an additional function associated with  $\epsilon_3 = 0.041$ . The form of this function (see Figure 3) is slightly more complex, but it is interesting to observe that it is again localized in the region of the adjacent lithium triangle.

The above description of the bonding is straightforwardly corroborated by the SEDI values calculated for the RHF and full-valence CASSCF levels of theories (see Table 1). Examination of the various numerical values does indeed suggest that much of the electron sharing is localized within triangles Li<sub>1</sub>Li<sub>2</sub>Li<sub>3</sub> and Li<sub>1</sub>Li<sub>2</sub>Li<sub>4</sub> but that it does not in fact come predominantly from interactions between the lithium atoms. The largest contributions arise instead from sharing between the atomic domains of the lithium triangle and the domain of the corresponding non-nuclear attractor. As a consequence, the bonding in the Li<sub>4</sub> cluster can be regarded as being composed of two 4-center 2-electron bonding units associated with the

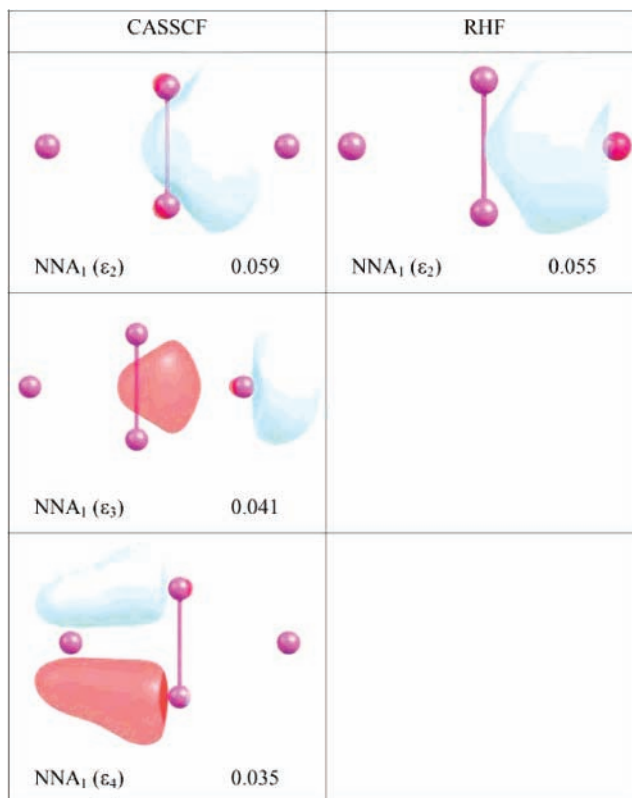


**Figure 3.** Additional DAFH eigenvectors associated with the NNA domains of the Li<sub>4</sub> cluster.

Li<sub>1</sub>Li<sub>2</sub>Li<sub>3</sub>NNA<sub>1</sub> and Li<sub>1</sub>Li<sub>2</sub>Li<sub>4</sub>NNA<sub>2</sub> moieties, with the sharing of electrons between these two subunits. Some indication of the extent of the sharing between the two parts of the molecule is provided by values of the quantity SEDI( $\Omega_\alpha, \Omega_\beta$ ) (see Table 1), in which  $\Omega_\alpha \equiv \text{Li}_3\text{NNA}_1$  and  $\Omega_\beta \equiv \text{Li}_4\text{NNA}_2$ . We note also that whereas the various numerical values for lithium domains are consistent with the usual expectations that the inclusion of electron correlation generally leads to an increase in the degree of localization of electrons in atomic domains, with a simultaneous reduction in the extent of sharing between domains, the opposite behavior is observed here for the NNA domains.

Given that two-electron density matrices are not available to us for the B3LYP treatment of this cluster, we are, of course, unable to calculate 'genuine' B3LYP SEDI values. However, in the spirit of a number of previous studies, we have reported in Table 1 the 'pseudo-B3LYP' results which may be obtained simply by putting the RKS orbitals into the simplified expression for  $g_B(\mathbf{r}_1)$  that applies for RHF wave functions (as was explained earlier, in the context of H<sub>2</sub>). On the whole, we observe that some of the pseudo-B3LYP SEDI values are somewhat closer to the RHF results than we might have wished, and the differences from the RHF values are somewhat erratic, not being consistently in the direction of the CASSCF results. We also find that the analogous pseudo-B3LYP DAFH analysis produces one-electron functions  $f_i$  that most closely resemble those generated at the RHF level, with the same apparent lack of flexibility in the functions associated with the domains of atoms Li<sub>1</sub> and Li<sub>2</sub>. Ultimately, of course, these self-evident limitations of such pseudo-B3LYP values are not at all surprising: it is entirely unrealistic to expect an intrinsically one-electron approach such as RKS to take proper account of electron correlation effects in the calculation of a two-particle density matrix. Far more promising in this respect are models based, for example, on two-electron phase-space information.<sup>19</sup>

**TABLE 2:  $R$ -Dependence of Valence Electron Populations ( $q$ ), Shared-Electron Distribution Indices (SEDI), and Localization Indices ( $k$ ) for AIM Domains in the  $\text{Li}_2$  Molecule**

$R/\text{\AA}$	$q(\text{Li}_1)$	$q(\text{NNA})$	SEDI ( $\text{Li}_1, \text{Li}_2$ )	SEDI ( $\text{Li}_1, \text{NNA}$ )	$k(\text{Li}_1, \text{Li}_1)$	$k(\text{NNA}, \text{NNA})$
2.0	1.000		0.839		0.580	
2.1	0.479	1.042	0.150	0.492	0.158	0.552
2.4	0.483	1.033	0.142	0.488	0.168	0.545
2.7	0.526	0.948	0.150	0.487	0.207	0.461
3.0	0.617	0.766	0.182	0.463	0.293	0.304
3.3	0.763	0.474	0.262	0.359	0.452	0.116
3.4	1.000		0.587		0.707	
4.0	1.000		0.422		0.789	

$\text{Li}_2$ . The relatively weak and relatively long bond in  $\text{Li}_2$  is also associated with a non-nuclear attractor (NNA). As the two neutral atoms are brought together, there is a catastrophic change in the topology of the total electron density,<sup>7</sup> with the sudden appearance of the NNA at the center of the molecule. Of course, the precise range of nuclear separations  $R$  for which this NNA occurs depends on the quality of the electron density being analyzed. In the present work, a non-nuclear attractor was observed in our calculations for 2.1–3.3 Å, but it was absent at a shorter distance (2.0 Å) and at a long one (3.4 Å), for which we found instead only the expected domains associated with individual lithium atoms.

The observed change in the number of AIM domains has, of course, a dramatic impact on the values of the calculated domain populations  $q$  for the valence electrons (Table 2). The creation of the NNA results in a significant depletion of electron density from the lithium domains and its accumulation in the domain of the NNA. Indeed, the electron population of the NNA domain can exceed the population of individual lithium domains (for the valence electrons). This implies that the nature of the electron sharing in this molecule will be very different from that in, say,  $\text{H}_2$ .

We find for all the  $R$  values that we considered that DAFH analysis for each domain yields just one dominant eigenvalue. The most dramatic changes with bond length in the forms of the corresponding functions (see Figure 4) occur for the lithium domains, which resemble the  $\text{Li}_2$   $2\sigma_g$  orbital at short  $R$  but show increasing localization at large  $R$ , so as to take the form of  $\text{Li}(2s)$  at dissociation. On the other hand, the shape of the corresponding function for the NNA shows much less sensitivity to  $R$ , over the range of distances for which it occurs.

All in all, the DAFH analysis suggests that the most important effect of the participation of the NNA is that it dramatically changes the pattern of electron sharing such that the conventional sharing between atoms is considerably reduced in favor of the sharing between the domain of the NNA and the domains of the individual lithium atoms. The values of the SEDI indices, that characterize quantitatively the extent of such sharing, are summarized in Table 2. The importance of the NNA in the description of the bonding can also be seen from Figure 5 which shows the  $R$ -dependence of the sum of  $\text{SEDI}(\text{Li}_1, \text{Li}_2)$  and  $\text{SEDI}(\text{Li}_1, \text{NNA})$ , which takes into account the combined effect of the different types of sharing in the molecule. In the case of ordinary homopolar bonds that are not complicated by the presence of NNAs, the splitting of the bond is straightforwardly reflected in a systematic monotonic decrease of the extent of electron sharing with increasing  $R$ .<sup>4,5</sup> As can be seen from Figure 5, the  $R$ -dependence for the valence electrons of  $\text{Li}_2$  is entirely different, in that the total extent of electron sharing appears to be relatively constant within the range of nuclear separations for which the NNA is present in the electron density. Only for

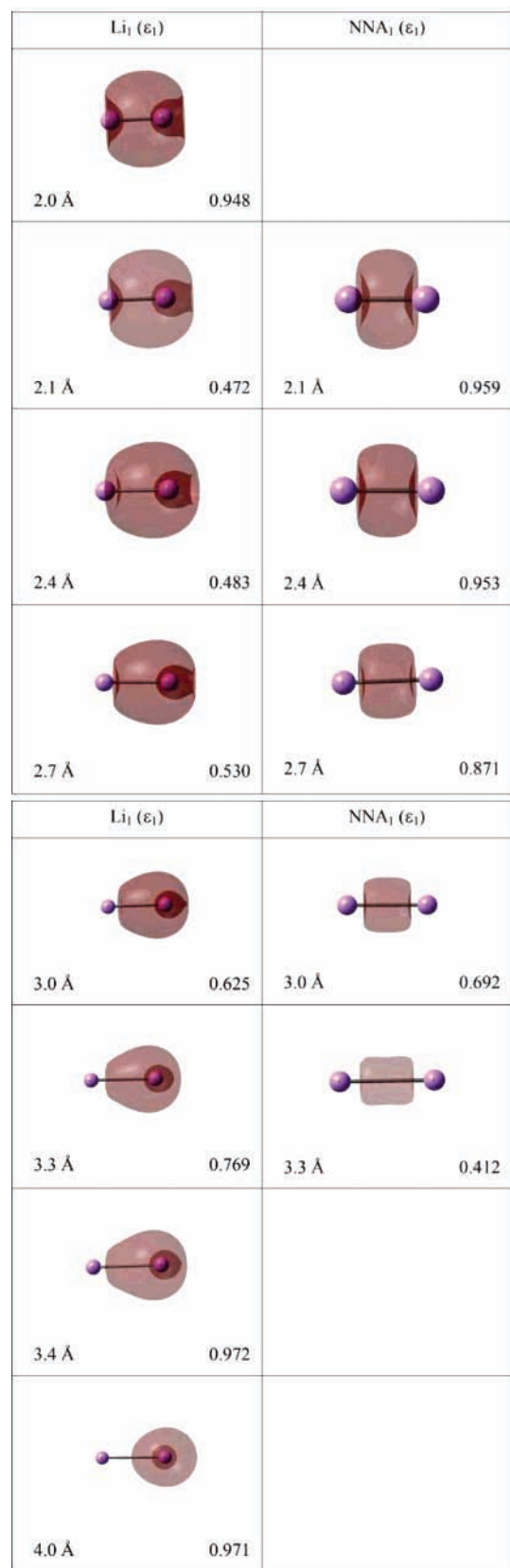


**Figure 4.** Bond dissociation monitored by the  $R$ -dependence of DAFH eigenvectors associated with the domains of a Li atom and the NNA in  $\text{Li}_2$ . The displayed isovalue for the left-hand column is 0.04 and for the right-hand column it is 0.06.

larger  $R$ , after the disappearance of the NNA, do the SEDI values show a more conventional decline with increasing nuclear separation.

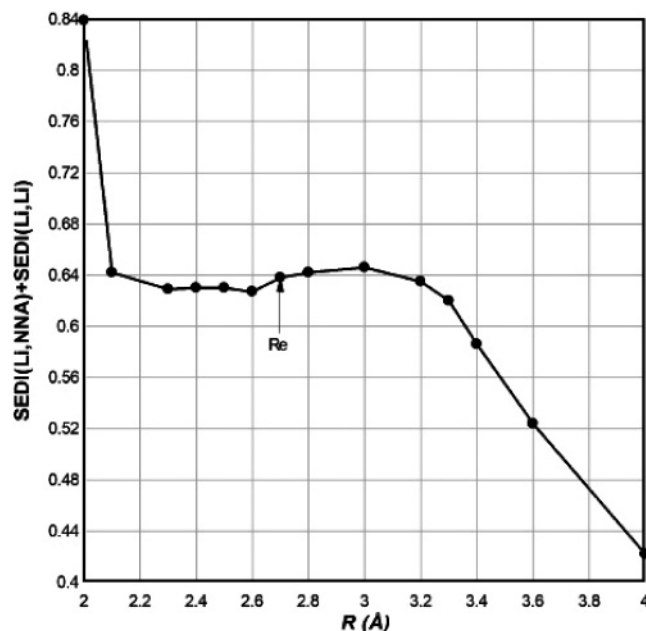


**Figure 5.**  $R$ -dependence of the total extent of valence electron sharing in  $\text{Li}_2$ , as characterized by the sum of SEDI indices for both types of sharing with one of the lithium atoms.

**TABLE 3:  $R$ -Dependence of the Numerical Values and Degeneracies of the (Transformed) Eigenvalues  $\epsilon_i$  from the DAFH Analysis for an F Atom in the  $\text{F}_2$  Molecule**

$R/\text{Å}$	$\epsilon_i$	interpretation	$R/\text{Å}$	$\epsilon_i$	interpretation
1.25	1.984 (1×)	$\sigma$ -like lone pair	1.60	1.985 (1×)	$\sigma$ -like lone pair
	1.966 (2×)	$\pi$ -like lone pairs		1.983 (2×)	$\pi$ -like lone pairs
	0.995 (1×)	free valence		0.989 (1×)	free valence
1.30	1.983 (1×)	$\sigma$ -like lone pair	1.75	1.988 (1×)	$\sigma$ -like lone pair
	1.969 (2×)	$\pi$ -like lone pairs		1.988 (2×)	$\pi$ -like lone pairs
	0.994 (1×)	free valence		0.988 (1×)	free valence
1.40	1.983 (1×)	$\sigma$ -like lone pair	2.25	1.996 (1×)	$\sigma$ -like lone pair
	1.975 (2×)	$\pi$ -like lone pairs		1.995 (2×)	$\pi$ -like lone pairs
	0.992 (1×)	free valence		0.995 (1×)	$2p_z$
1.50	1.983 (1×)	$\sigma$ -like lone pair	2.50	1.998 (1×)	$\sigma$ -like lone pair
	1.979 (2×)	$\pi$ -like lone pairs		1.996 (2×)	$\pi$ -like lone pairs
	0.990 (1×)	free valence		0.998 (1×)	$2p_z$

$\text{F}_2$ . This molecule provides a somewhat different example of a relatively weak homopolar bond. This last has often been attributed to the repulsive interaction inherent in the so-called lone-pair bond weakening effect (LPBWE).<sup>20,21</sup> The weakened nature of the bonding is certainly evident in AIM analysis, for which positive values of the Laplacian indicate the depletion of electron density from the bonding region, in contrast to what is usually observed for ordinary covalent bonds.<sup>22</sup> The LPBWE explanation is not, however, supported by the results of an energy decomposition analysis (EDA) scheme<sup>23</sup> which suggests that the Pauli repulsion term for  $\text{F}_2$  is in fact smaller than for  $\text{O}_2$  and even for  $\text{N}_2$ . Instead, the EDA results suggest that the weakened bond in  $\text{F}_2$  is associated primarily with poor electrostatic attraction. Yet another rationalization of the unusual bonding in this molecule, albeit inherently tied to a particular type of construction for the wave function, invokes instead the notion of ionic-covalent resonance.<sup>24</sup>

Whatever the preferred explanation for the relatively weak bonding in  $\text{F}_2$ , it is important to investigate the extent to which DAFH analysis can distinguish the bonding in  $\text{F}_2$  from that in (say)  $\text{H}_2$ , preferably without having to resort to very high quality wave functions. It would indeed be a failure of the methodology if there were no clear indications in the DAFH analysis that  $\text{F}_2$  is in some sense ‘different’. It is difficult to predict in advance

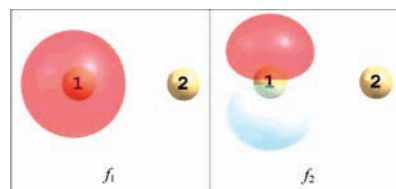


**Figure 6.** DAFH eigenvectors corresponding to nonbonding orbitals on an F atom in the  $\text{F}_2$  molecule for a bond length of 1.50 Å. Displayed isovalue: 0.12.

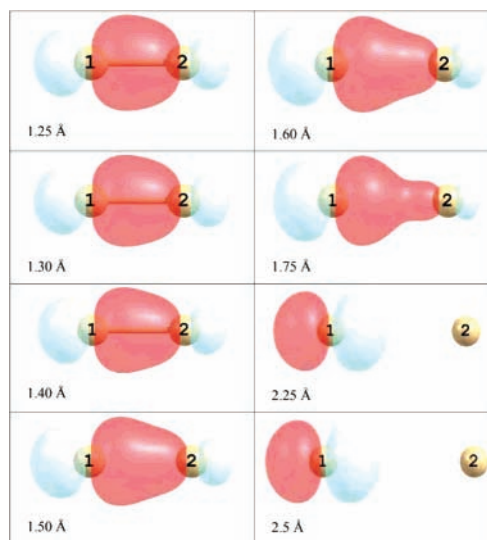


**Figure 7.** Dissociation of the F–F bond monitored by the  $R$ -dependence of DAFH eigenvectors corresponding to the broken valence associated with one of the F atoms in  $\text{F}_2$ . Displayed isovalue: 0.12.

of performing the calculations how  $\text{F}_2$  might manifest the weakened bond in the DAFH analysis.

As mentioned previously, the full-valence CASSCF wave functions employed here for a set of internuclear distances ranging from 1.25 Å to 2.50 Å are of rather modest quality. In particular, the lowest calculated energy occurred for 1.5 Å, whereas the experimental equilibrium bond length is 1.412 Å. These calculations should, however, be more than adequate for our present purposes.

DAFH analysis for the domain of one of the F atoms yields in all cases four dominant eigenvalues, of which three are close to 2 and the remaining one is close to 1. As can be seen from Table 3, these values vary relatively little with  $R$ . In accordance with previous experience for systems with nonbonding electrons, the eigenvalues close to 2 are likely to be associated with fluorine lone pairs. Such an interpretation is straightforwardly corroborated by inspection of the form of the corresponding functions (see Figure 6): we observe one  $\sigma$ -like and two  $\pi$ -like lone pairs on fluorine. The basic form of these functions is much the same for all  $R$ .

It is tempting to interpret the remaining dominant eigenvalue, close to 1, as the ‘free valence’ function formed by symmetrical splitting of the bonding electron pair of the homopolar F–F bond. Such an interpretation is again straightforwardly corroborated by inspection of the corresponding functions (see Figure 7). Consistent with conventional expectations, the splitting of the F–F bond is reflected in a smooth transformation of the ‘free valence’ function from a more or less symmetrical form, reminiscent of a  $\sigma_g$  orbital, to the appropriate  $2p_z$  atomic orbital localized on the corresponding atom at the dissociated limit.

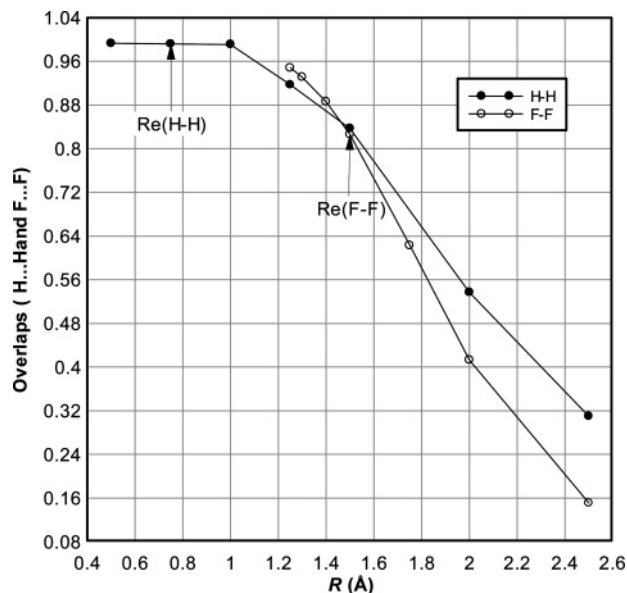


**Figure 8.**  $R$ -dependence of the overlaps of the DAFH eigenvalues associated with the free valences of the individual atomic domains in  $H_2$  and  $F_2$ .

Whereas for a molecule such as  $H_2$  the equilibrium geometry occurs in the range of  $R$  for which the DAFH function is still fairly symmetrical, a certain degree of asymmetry is already more apparent in the case of  $F_2$ . Analogous comparisons with other systems also show  $F_2$  to be unusual. Even so, the inferences from such visual inspection of the relevant figures are rather subjective. As such, it is more useful to consider numerical analysis of these functions. Specifically, we examine, for a given bond length, the overlap between the DAFH functions for the different domains in the molecule. When these functions are highly symmetrical, as occurs for short  $R$ , this overlap will approach unity, but as the functions become more localized at larger  $R$ , this overlap will tend to zero, in much the same fashion as a bond order. These overlaps, for  $H_2$  and for  $F_2$ , are shown graphically in Figure 8. Whereas for  $H_2$  the equilibrium geometry corresponds to a region of the graph in which this quantity shows very little tendency to decrease, the corresponding bond length for  $F_2$  (whether the calculated or experimental value) is located in the region for which this overlap is already decreasing fairly rapidly with increasing  $R$ . This suggests that the observed weakness of the F–F bond can, roughly speaking, be attributed in DAFH analysis to the notion that for  $R$  values close to equilibrium geometry the bond is already partly dissociated. In this way, the DAFH analysis clearly distinguishes  $F_2$  from more conventional homopolar bonds such as those we have considered previously. On the other hand, the  $R$ -dependence of the SEDI values (and localization indices) turns out to be much the same as has been observed for other bonds.

## 5. Conclusions

Domain-averaged Fermi hole (DAFH) analysis is a relatively new technique for the interpretation, visualization, and characterization of chemical bonding for correlated wave functions. We have demonstrated here that it can provide particular insights into the nature of the bonding in systems that feature one or more non-nuclear attractors (NNAs). DAFH analysis, coupled with an examination of (combinations of) SEDI values, shows that the sharing of valence electrons in the  $Li_4$  rhombus is not in fact dominated by direct interactions between the lithium

atoms. Instead, the largest contributions come from sharing between the individual atomic domains of a lithium triangle and the domain of the corresponding NNA, as well as electron sharing between these two 4-center 2-electron bonding units.

In the case of  $Li_2$ , we used DAFH analysis (and SEDI values) to monitor the electron reorganization that accompanies bond splitting. For an extended range of nuclear distances  $R$ , the total electron density features a non-nuclear attractor at the center of the molecule. For those geometries, the conventional pattern of electron sharing between atoms is considerably reduced in favor of sharing between the domain of the NNA and the domains of the individual lithium atoms. Furthermore, the total extent of valence electron sharing in  $Li_2$  appears to be relatively constant within the range of  $R$  for which the NNA is present. Only for larger  $R$ , after the disappearance of the NNA, do the SEDI values show a more conventional decline with increasing nuclear separation that is more typical of ordinary homopolar bonds that are not complicated by the presence NNAs.

We also examined how the weakened bonding in  $F_2$  might manifest itself in DAFH analysis. In the case of  $H_2$ , the DAFH functions are still fairly symmetrical for  $R$  values close to equilibrium geometry, but they do, of course, localize onto a single center as the bond is broken. For  $F_2$ , on the other hand, the DAFH functions already show somewhat more asymmetry near equilibrium geometry, which corresponds to a region in which the overlap between the DAFH functions for the two domains is already decreasing significantly with increasing  $R$ .

We have shown for  $H_2$ , albeit in a modest basis set, that the inclusion of dynamical electron correlation makes only small quantitative differences to the DAFH analysis relative to a somewhat cheaper calculation that mostly includes only non-dynamical correlation. The basic descriptions are much the same. Far less successful, for  $H_2$  and for  $Li_4$ , is the so-called ‘pseudo-RKS’ scheme. As was to be expected, it proves difficult to argue that inserting RKS orbitals into the simplified expression that applies for the RHF level takes proper account of key correlation effects. There is, of course, nothing surprising about these observations, but we believe that it was useful to be able to demonstrate the extent of the limitations due to such pseudo-RKS manipulations, which are still being fairly widely used in the literature. Of course, the downside of wanting to perform instead the full calculation, without such approximations, is that the required pair densities are not always so readily available.

Taken together with our previous studies,<sup>4,5</sup> the various results presented here provide significant confidence that DAFH analysis of correlated wave functions is very likely to furnish useful new insights for a wide range of chemical systems.

## References and Notes

- (1) Bader, R. F. W. *Atoms in Molecules. A Quantum Theory*; Clarendon Press: Oxford, U.K. 1994.
- (2) Silvi, B.; Savin, A. *Nature* **1994**, *371*, 683.
- (3) Weinhold, F.; Landis, C. *Valency and Bonding: A Natural Bond Order Donor-Acceptor Perspective*; Cambridge University Press: Cambridge, U.K. 2005.
- (4) Ponec, R.; Cooper, D. L. *Faraday Discuss.* **2007**, *135*, 31.
- (5) Ponec, R.; Cooper, D. L. *J. Mol. Struct. (THEOCHEM)* **2005**, *727*, 133.
- (6) (a) Gatti, C.; Fantucci, P.; Pacchioni, G. *Theor. Chem. Acta* **1987**, *72*, 433. (b) Cao, W. L.; Gatti, C.; MacDougall, P. J.; Bader, R. F. W. *Chem. Phys. Lett.* **1987**, *141*, 380.
- (7) (a) Cioslowski, J. *J. Phys. Chem.* **1990**, *94*, 5496. (b) Cooper, D. L. *Nature* **1990**, *346*, 796. (c) Bersuker, G. I.; Peng, C.; Boggs, J. E. *J. Phys. Chem.* **1993**, *97*, 9323. (d) Penotti, F. E. *Int. J. Quantum Chem.* **2000**, *78*, 378.
- (8) (a) Ponec, R. *J. Math. Chem.* **1997**, *21*, 323. (b) Ponec, R. *Math. Chem.* **1998**, *23*, 1083. (c) Ponec, R.; Duben, A. J. *J. Comput. Chem.* **1998**, *20*, 760. (d) Ponec, R.; Roithová, J.; Gironés, X.; Lain, L.; Torre, A.;

- Bochicchio, R. *J. Phys. Chem. A* **2002**, *106*, 1019. (e) Ponec, R.; Gironés, X. *J. Phys. Chem. A* **2002**, *106*, 9506. (f) Ponec, R.; Yuzhakov, G.; Carbó-Dorca, R. *J. Comput. Chem.* **2003**, *24*, 1829. (g) Ponec, R.; Yuzhakov, G.; Gironés, X.; Frenking, G. *Organometallics* **2004**, *23*, 1790. (h) Ponec, R.; Yuzhakov, G.; Cooper, D. L. *Theor. Chem. Acc.* **2004**, *112*, 419. (i) Ponec, R.; Yuzhakov, G.; Sundberg, M. R. *J. Comput. Chem.* **2005**, *26*, 447.
- (9) McWeeny, R. *Rev. Mod. Phys.* **1960**, *32*, 335.
- (10) Cioslowski, J. *Int. J. Quantum Chem.* **1990**, *S24*, 15.
- (11) Fradera, X.; Austen, M. A.; Bader, R. F. W. *J. Phys. Chem. A* **1999**, *103*, 304.
- (12) Gillespie, R. J.; Bayles, D.; Platts, J.; Heard, G. L.; Bader, R. W. F. *J. Phys. Chem. A* **1998**, *102*, 3407.
- (13) Bader, R. W. F.; Heard, G. L. *J. Chem. Phys.* **1999**, *111*, 8789.
- (14) Geier, J. *J. Phys. Chem. A* **2006**, *110*, 9273.
- (15) Guest, M. F.; Sherwood, P. *GAMESS-UK User's Guide and Reference Manual, Revision B.0*; SERC Daresbury Laboratory: Daresbury, U.K., 1992.
- (16) Amos, R. D.; Bernhardsson, A.; Berning, A.; Celani, P.; Cooper, D. L.; Deegan, M. J. O.; Dobbyn, A. J.; Eckert, F.; Hampel, C.; Hetzer, G.; Knowles, P. J.; Korona, T.; Lindh, R.; Lloyd, A. W.; McNicholas, S. J.; Manby, F. R.; Meyer, W.; Mura, M. E.; Nicklass, A.; Palmieri, P.; Pitzer, R.; Rauhut, G.; Schütz, M.; Schumann, U.; Stoll, H.; Stone, A. J.; Tarroni, R.; Thorsteinsson, T.; Werner, H.-J. MOLPRO, a package of ab initio programs designed by H.-J. Werner and P. J. Knowles, version 2002.10.
- (17) Dunning, T. H., Jr. *J. Chem. Phys.* **1971**, *55*, 716.
- (18) Rao, B. K.; Jena, P. *Phys. Rev. B* **1985**, *32*, 2058.
- (19) Gill, P. M. W.; Crittenden, D. L.; O'Neill, D. P.; Besley, N. A. *Phys. Chem. Chem. Phys.* **2006**, *8*, 15.
- (20) Schwartz, W. H. E.; Valtazanos, P.; Ruedenberg, K. *Theor. Chim. Acta* **1985**, *68*, 471.
- (21) Sanderson, R. *Polar Covalence*; Academic Press: New York, 1983.
- (22) Cremer, D.; Kraka, E. *Angew. Chem., Int. Ed. Engl.* **1984**, *23*, 627.
- (23) Krapp, A.; Bickelhaupt, F. M.; Frenking, G. *Chem. Eur. J.* **2006**, *12*, 9196.
- (24) Hiberty, P. C.; Ramozzi, R.; Song, L.; Wu, W.; Shaik, S. *Faraday Discuss.* **2007**, *135*, 261.